

M-GenSeg: Domain Adaptation For Target Modality Tumor Segmentation With Annotation-Efficient Supervision

Malo de Boisredon¹, Eugene Vorontsov², and Samuel Kadoury¹

¹ Ecole Polytechnique de Montréal

² Paige

Abstract. Automated medical image segmentation using deep neural networks typically requires substantial supervised training. However, these models fail to generalize well across different imaging modalities. This shortcoming, amplified by the limited availability of annotated data, has been hampering the deployment of such methods at a larger scale across modalities. To address these issues, we propose M-GenSeg, a new semi-supervised training strategy for accurate cross-modality tumor segmentation on unpaired bi-modal datasets. Based on image-level labels, a first unsupervised objective encourages the model to perform diseased to healthy translation by disentangling tumors from the background, which encompasses the segmentation task. Then, teaching the model to translate between image modalities enables the synthesis of target images from a source modality, thus leveraging the pixel-level annotations from the source modality to enforce generalization to the target modality images. We evaluated the performance on a brain tumor segmentation datasets composed of four different contrast sequences from the public BraTS 2020 challenge dataset. We report consistent improvement in Dice scores on both source and unannotated target modalities. On all twelve distinct domain adaptation experiments, the proposed model shows a clear improvement over state-of-the-art domain-adaptive baselines, with absolute Dice gains on the target modality reaching 0.15.

Keywords: Image Segmentation · Semi-supervised Learning · Unpaired Image-to-image Translation.

1 Introduction

Deep learning methods have demonstrated their tremendous potential when it comes to medical image segmentation. However, the success of most existing architectures relies on the availability of pixel-level annotations, which are difficult to produce [1]. Furthermore, these methods are known to be inadequately equipped for distribution shifts. One example is for cross-modality generalization, which is useful when one imaging modality has insufficient training data. For instance, it could be required in segmentation tasks where annotations are sufficiently available for T1 and T2 images but lacking in other MRI sequences. This challenge can be addressed through semi-supervised domain-adaptive approaches, which learn to transfer the knowledge available in

the “source” modality from pixel-level labels to the “target” imaging modality lacking annotations [2].

Several strategies can be employed to address the modality adaptation problem. For instance, generative models attempt to generalize to a target modality by performing unsupervised domain adaptation through image-to-image translation and image reconstruction. In [3], by learning to translate between CT and MR cardiac images, the proposed model would jointly disentangle the domain specific and domain invariant features between each modality and train a segmenter from the domain invariant features, which can then be applied to the target modality. Other methods [4,5,6,7,8] also integrate this translation approach, but the segmenter is trained in an end-to-end manner, on the synthetic target images generated from the source modality using a CycleGAN [9] model. While these methods perform well, they depend on the availability of pixel-level annotations for source modality images.

In this paper, we propose M-GenSeg, a novel training strategy as illustrated in Fig. 1, which achieves domain adaptation from a partially unannotated source modality to an unannotated target modality. This work extends GenSeg [10], a training method that uses image-level “diseased” or “healthy” labels for semi-supervised segmentation. Given these labels, the model imposes an image-to-image translation objective between the image domain presenting tumor lesions and the domain corresponding to an absence of lesions. Teaching the model to find and remove a tumor guides the model to segment the tumor. We incorporate cross-modality image segmentation by adding a second unsupervised objective: an image-to-image translation between source and target modalities. We hypothesize both objectives are complementary since GenSeg helps localizing the tumor on target images, while modality translation enables fine-tuning the segmentor on the target modality by displaying synthetic labelled target images. We evaluate M-GenSeg on a modified version of the BraTS 2020 dataset, in which each type of sequence (T1, T2, T1ce and FLAIR) is considered as a distinct modality. We demonstrate that our model can better generalize than other methods to the target modality. Furthermore, M-GenSeg is semi-supervised in the source modality.

2 Methods

2.1 M-GenSeg : semi-supervised segmentation

Healthy-diseased translation. The objective of this work is learn to localize and segment tumor lesions in a target modality by making efficient use of the image-level labels via a generative model. The latter introduces translation between presence and absence (of tumor lesions) domains, referred as P and A. This requires disentangling the information common to A and P, and the one specific to P. For this purpose, we split the latent representation of each image into two distinct codes \mathbf{c} , \mathbf{u} that respectively refer to common and unique codes. Basically, the common code contains information inherent to both domains, which represents organs and other structures, while the unique code stores features like tumor shapes and localization.

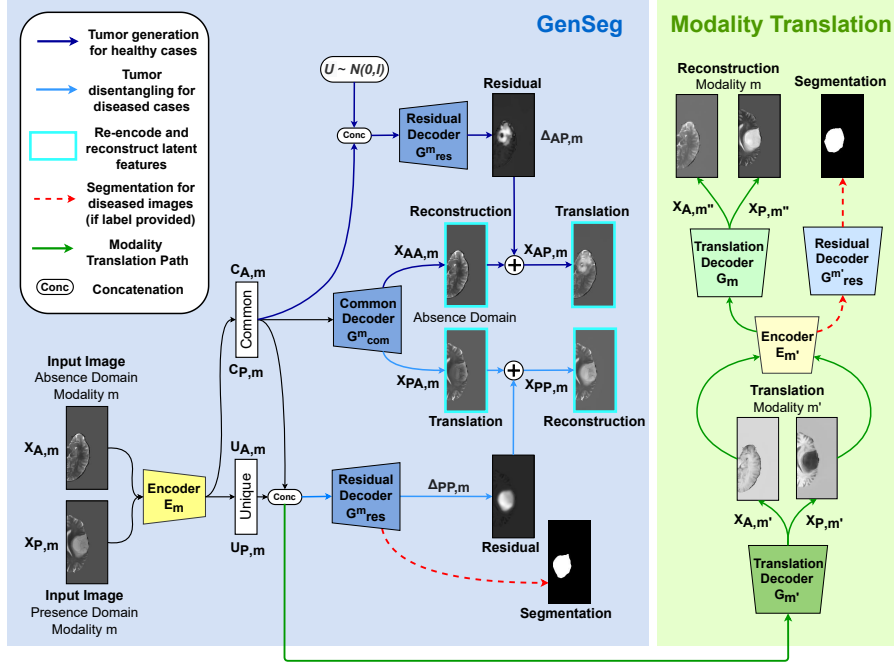


Fig. 1: M-GenSeg: Simultaneous domain adaptation and semi-supervised segmentation. The common code is used by common decoders for either absence to presence translation or image reconstruction. Both segmentation and tumor disentangling are performed on diseased inputs by residual decoders. The latter also generates synthetic residuals for absence to presence translation, after sampling from a normal distribution. Finally, based on the same latent representation, cross-modality transposition is performed in a CycleGan-like approach.

Presence to absence translation. Given an image of modality m in the presence domain $x_{P,m}^m$, we use an encoder E_m to compute the latent representation $[c_{P,m}^m, u_{P,m}^m]$. A common decoder G_{com}^m takes as input the common code $c_{P,m}^m$ and generates a healthy version $x_{PA,m}^m$ of that image by removing the apparent tumor region. Simultaneously, both common and unique codes are used by a residual decoder G_{res}^m to output a residual image $\Delta_{PP,m}^m$, which corresponds to the additive change necessary to shift the generated healthy image back to the presence domain. In other words, the residual is the disentangled tumor that can be added to the generated healthy image to create a reconstruction $x_{PP,m}^m$ of the initial diseased image:

$$x_{PA,m}^m = G_{com}^m(c_{P,m}^m), \quad (1)$$

$$\Delta_{PP,m}^m = G_{res}^m(c_{P,m}^m, u_{P,m}^m), \quad (2)$$

$$x_{PP,m}^m = x_{PA,m}^m + \Delta_{PP,m}^m. \quad (3)$$

Absence to presence translation. Concomitantly, a similar path is achieved for images in the healthy domain. Given an image $x_{A,m}^m$ of modality m in domain

A, we generate a translated version in domain P. To do so, a synthetic tumor Δ_{AP}^m is generated by sampling a code from the normal distribution $\mathcal{N}(0, \mathbf{I})$ and replacing the encoded unique code for that image. The reconstruction of the original image in domain A and the synthetic diseased image x_{AP}^m in domain P are computed from the encoded features $[\mathbf{c}_A^m, \mathbf{u}_A^m]$ as follows:

$$\mathbf{x}_{AA}^m = G_{com}^m(\mathbf{c}_A^m), \quad (4)$$

$$\mathbf{x}_{AP}^m = \mathbf{x}_{AA}^m + G_{res}^m(\mathbf{c}_A^m, \mathbf{u} \sim \mathcal{N}(0, \mathbf{I})). \quad (5)$$

There are multiple ways a tumor can appear in the brain. Presence \rightarrow Absence translation thus requires a one-to-many mapping, here enabled by sampling the unique code in a normal distribution. It is important to note that translating from Absence \rightarrow Presence domain performs indirect data augmentation, thus improving segmentation performance. Finally, in both translation directions we reconstruct the latent representations of the generated images, to ensure that the translation task holds the information relative to the initial image. In the Absence \rightarrow Presence direction, it notably enforces that the distribution of unique codes matches with the prior.

Modality translation. While the GenSeg framework handles primarily the segmentation of tumors, it is done only in the source modality. Indeed, for each modality m , the segmenter G_{seg}^m shares most of its weights with the residual decoder, but has its own set of normalization parameters and a supplementary classifying layer. Thus, through the Absence and Presence translations, the segmenters have already learned how to disentangle the tumor from the background. However, supervised training on a few example annotations is still required to learn how to transform the resulting residual representation into appropriate segmentation maps. While this is a fairly straightforward task for the source modality using pixel-level annotations, achieving this for the target modality requires further efforts, justifying the second unsupervised translation objective between source and target modalities. Based on the CycleGan [9] approach, modality translations are performed via two distinct generators that share their encoder with the GenSeg task. More precisely, two different decoders G_S and G_T respectively perform the decoding towards source and target modalities. Lastly, given an image \mathbf{x}_b^m of modality $m \in \{S, T\}$ in domain $b \in \{P, A\}$, and m' the other modality, we perform a cyclic translation by generating $\mathbf{x}_d^{m'}$ in domain m' and $\mathbf{x}_d^{m''}$ a reconstruction of the original image:

$$[\mathbf{c}_b^m, \mathbf{u}_b^m] = E_m(\mathbf{x}_b^m), \quad (6)$$

$$\mathbf{x}_b^{m'} = G_{m'}(\mathbf{c}_b^m, \mathbf{u}_b^m) = [G_{m'} \circ E_m](\mathbf{x}_b^m), \quad (7)$$

$$[\mathbf{c}_b^{m'}, \mathbf{u}_b^{m'}] = E_{m'}(\mathbf{x}_b^{m'}), \quad (8)$$

$$\mathbf{x}_b^{m''} = G_m(\mathbf{c}_b^{m'}, \mathbf{u}_b^{m'}) = [G_m \circ E_{m'}](\mathbf{x}_b^{m'}) = [G_m \circ E_{m'} \circ G_{m'} \circ E_m](\mathbf{x}_b^m). \quad (9)$$

Modality translation is only required on source images that have pixel-level annotations. However, performing translation on all types of images and in both directions yield additional training examples for modality generators. Ultimately, modality translation enables to fine-tune the segmentor on annotated

synthetic target images, generated from the source images that possess pixel-level annotations \mathbf{y}_S . Based on (i) the encoded features $[\mathbf{c}_P^S, \mathbf{u}_P^S]$ of an original source image in domain P, (ii) and the latent representation $[\mathbf{c}_P^T, \mathbf{u}_P^T]$ of its translation to target modality, two segmentation masks for that image are generated:

$$\hat{\mathbf{y}}_S = G_{seg}^S(\mathbf{c}_P^S, \mathbf{u}_P^S), \quad (10)$$

$$\hat{\mathbf{y}}_T = G_{seg}^T(\mathbf{c}_P^T, \mathbf{u}_P^T). \quad (11)$$

By sharing the latent space between segmentation and modality translation tasks, M-GenSeg is forced to learn a common representation relevant to both of them, which can then be interpreted separately by the different decoders. Furthermore, because \mathbf{u} is sampled from a single prior for the healthy to diseased translation, one can expect that: (i) modality information cannot be encoded in \mathbf{u} , (ii) modality must be encoded in \mathbf{c} , (iii) residual and translation decoders interpret which features in \mathbf{u} to visualize, and how, based on the code in \mathbf{c} .

2.2 Loss functions

Segmentation Loss. For the segmentation objective, we compute a soft Dice loss [11] on the predictions for both labelled source images and their translations:

$$\mathcal{L}_{seg} = Dice(\mathbf{y}_S, \hat{\mathbf{y}}_S) + Dice(\mathbf{y}_S, \hat{\mathbf{y}}_T). \quad (12)$$

Reconstruction Losses. We impose pixel level image reconstruction constraints on both modality translation task:

$$\mathcal{L}_{cyc}^{mod} = \sum_{\substack{m \in \{S, T\} \\ b \in \{A, P\}}} \mathcal{L}_1(\mathbf{x}_b^{m''}, \mathbf{x}_b^m), \quad (13)$$

and GenSeg task:

$$\mathcal{L}_{rec}^{Gen} = \sum_{m \in \{S, T\}} [\mathcal{L}_1(\mathbf{x}_{AA}^m, \mathbf{x}_A^m) + \mathcal{L}_1(\mathbf{x}_{PP}^m, \mathbf{x}_P^m)]. \quad (14)$$

Likewise, we enforce the images generated in the GenSeg path to have distributions that match across presence and absence domains by reconstructing their latent codes.

$$\begin{aligned} \mathcal{L}_{lat}^{Gen} = & \sum_{m \in \{S, T\}} \mathcal{L}_1(E_m(\mathbf{x}_{AA}^m)|_{\mathbf{c}}, E_m(\mathbf{x}_A^m)|_{\mathbf{c}}) + \mathcal{L}_1(E_m(\mathbf{x}_{PA}^m)|_{\mathbf{c}}, E_m(\mathbf{x}_P^m)|_{\mathbf{c}}) \\ & + \mathcal{L}_1(E_m(\mathbf{x}_{AP}^m)|_{\mathbf{c}, \mathbf{u}}, [E_m(\mathbf{x}_A^m)|_{\mathbf{c}}, \mathbf{u}]) + \mathcal{L}_1(E_m(\mathbf{x}_{PP}^m)|_{\mathbf{c}, \mathbf{u}}, E_m(\mathbf{x}_P^m)|_{\mathbf{c}, \mathbf{u}}). \end{aligned} \quad (15)$$

Adversarial Loss. Lastly, we compute a hinge loss on real images \mathbf{x}_b and generated images $\hat{\mathbf{x}}_b$, for domains $b \in \{SA, SP, TA, TP\}$ in the GenSeg path.

$$\begin{aligned} \mathcal{L}_{adv}^{Gen} = & \sum_{b \in \{SA, SP, TA, TP\}} \min_G \max_D [-\mathbb{E}_{\mathbf{x}_b}(\min(0, D_b(\mathbf{x}_b) - 1)) \\ & - \mathbb{E}_{\hat{\mathbf{x}}_b}(\min(0, -D_b(\hat{\mathbf{x}}_b) - 1)) - \mathbb{E}_{\hat{\mathbf{x}}_b} D_b(\hat{\mathbf{x}}_b)] \end{aligned} \quad (16)$$

Likewise, a loss \mathcal{L}_{adv}^{mod} is computed on the modality translation path to generate synthetic images in source and target modalities.

Overall Loss. The overall loss for training M-GenSeg is a weighted sum of all the losses introduced above:

$$\begin{aligned} \mathcal{L}_{Total} = & \lambda_{seg} \mathcal{L}_{seg} + \lambda_{adv}^{mod} \mathcal{L}_{adv}^{mod} + \lambda_{cyc}^{mod} \mathcal{L}_{cyc}^{mod} \\ & + \lambda_{adv}^{Gen} \mathcal{L}_{adv}^{Gen} + \lambda_{rec}^{Gen} \mathcal{L}_{rec}^{Gen} + \lambda_{lat}^{Gen} \mathcal{L}_{lat}^{Gen}. \end{aligned} \quad (17)$$

To facilitate the hyper-parameter search, weights are normalized so that their sum always amounts to 1.

2.3 Implementation Details

Training and hyper-parameters Training and testing of the model were done in PyTorch. We used a batch size of 15 with the AMSGrad optimizer using β_1 and β_2 of 0.5 and 0.999 respectively, and a learning rate of 0.0001. Our models were trained for 300 epochs and weights of the segmentation model with the highest validation Dice score were saved for evaluation on the test set. The same on-the-fly data augmentation as in [10] was applied for all runs. Each training experiment was repeated three times for the baselines and M-GenSeg, with a different random seed for weight initialization. The performance reported is the mean of all test Dice mean scores, with standard deviation, across the three runs. We employed the following strategy to search for relative loss weights (λ in Eq. 17) : *(i)* with λ_{adv}^{Gen} , λ_{rec}^{Gen} and λ_{lat}^{Gen} set to zero, raise λ_{cyc}^{mod} with respect to λ_{adv}^{mod} until consistent modality translation and reconstruction enables adequate target modality segmentation; *(ii)* slowly incorporate GenSeg unsupervised components by increasing λ_{adv}^{Gen} , λ_{rec}^{Gen} and λ_{lat}^{Gen} so that consistent translation between presence and absence domains is achieved; *(iii)* and finally, fine tune λ_{seg} . We found that the following parameters yielded both great modality and absence/presence translations : $\lambda_{adv}^{mod} = 3$, $\lambda_{cyc}^{mod} = 20$, $\lambda_{adv}^{Gen} = 6$, $\lambda_{rec}^{Gen} = 20$ and $\lambda_{lat}^{Gen} = 2$. λ_{seg} varies depending on the fraction of pixel-level annotations provided to the network for training.

Architecture. Two distinct encoders, common decoders, residual and segmentation decoders, and modality translation decoders are used, one for each modality. In addition, four distinct discriminators are responsible for discriminating between real and synthetic samples for each of the four domains: Source/Presence, Source/Absence, Target/Presence and Target/Absence. Furthermore, modality translation should be independent from the presence and absence domains. Thus, we introduce two additional discriminators that are responsible for discriminating between real and synthetic images in source and target modalities respectively. The architecture used for encoders, decoders and discriminators is the same as in [10]. However, in order to better choose the semantic information relevant for each objective, we introduced attention gates [12] in the skip connections.

3 Experimental Results

3.1 Datasets

Experiments were performed on the BraTS 2020 challenge dataset, adapted for the multi-modal brain tumor segmentation problem where images are known

to be diseased (presence of tumors) or healthy (absence tumors). Amongst the 369 brain volumes available in BraTS, 37 were allocated for validation and test steps, while the 295 left were used for training. Based only on brain tissue, each brain volume was mean-centered and divided by five times the standard deviation. We then split the 3D brain volumes into 2 hemispheres and sliced them along the axial plane into 2D images. Then, slices where at least 1% of the brain surface came out to be tumors were labelled as diseased, while those that didn't show any tumor lesion were labelled as healthy images. Slices that didn't meet these criteria and those where less than 25% of the image was brain tissue were discarded. Also, to model the scenario of a bi-modal dataset, we picked source and target modalities out of the four MR contrasts available (T1, T2, T1ce and FLAIR) and discarded the slices corresponding to the two types of sequences left. To constitute unpaired training data, we used only one modality (source or target) per training volume. This was repeated for each possible pair of modalities. We could therefore experiment with twelve different combinations of unpaired source/target modalities. Finally, pixel-level ground-truth annotations were provided only for a portion of the diseased cases.

3.2 Model Evaluation

Domain adaptation. We compared M-GenSeg with AccSegNet [8] and AttENT [4], two high performance models for domain-adaptative medical image segmentation. To such an extent, we performed domain-adaptation experiments with source and target modalities drawn from T1, T2, FLAIR and T1ce. For each possible source/target pair, the images of source modalities were provided with pixel-level annotations, while the segmentation maps for target images were discarded. While our model outperforms both AccSegNet and AttENT by a slight margin on the source modality, it greatly improves the segmentation performance on target modality for all source/target pairs, as illustrated in Fig. 2. On average we report an absolute Dice score increase of 0.04 and 0.08 on target domain, respectively compared to AccSegNet and AttENT, with gain values reaching 0.15. We show in Fig. 5 several presence to absence translations and segmentation examples on different target modality images. As shown in the figure, although no pixel-level annotations were provided for the target modality, tumors were well disentangled from the brain, resulting in a successful presence to absence translation, and segmentation. Note that for T1 and T1ce sequences, where lesions are hypo-intense, M-GenSeg still manages to convert complex residuals into consistent segmentation maps.

Annotation deficit. We also tested M-GenSeg in scenarios with limited pixel-level annotations available in the source and target modalities. We trained models when only 1%, 10%, 40%, or 70% of the source modality and 0% of the target modality annotations were available, using T1 and T2 modalities and compared the performance to AccSegNet and AttENT. We also added the performance of two supervised methods without any domain adaptation, TransUnet [13] and a Unet with the same backbone architecture as the one used for M-GenSeg. Results are shown in Fig. 3. As expected, supervised methods trained on the source modality generalize poorly on the target modality.

However, even in the fully supervised setting (with 100% of the source images annotated), the semi-supervised M-GenSeg model performs better on the source modality than the Unet model with the same architecture. Thus, it appears that, similarly to UAGAN [14], the modality translation stream is helping to extract valuable features for the segmentation task. Also, the fact that TransUnet is outperforming M-GenSeg on the source modality for an annotation fraction above 40% indicates that the backbone architecture can be improved for our training strategy. Finally, these experiments show the robustness of our model in both the source and target modalities in a setting using a fraction of the annotated data. In both T1 to T2 and T2 to T1 adaptation experiments, while performance is severely dropping at 1% of annotations for the four baselines, our model shows in comparison only a slight decrease.

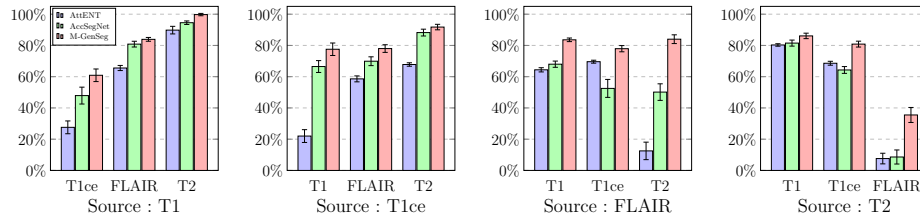


Fig. 2: Dice performance gap covered by each method on the target modality for each possible modality pair. At 0%, the model performs as poorly as supervised segmentation trained on source data without any domain adaptation strategy. At 100% it performs as well as UAGAN, a method designed for bi-modal datasets, trained on all of the source and target data.

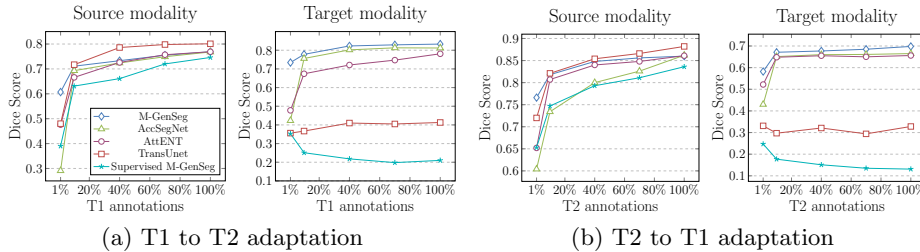


Fig. 3: Dice scores with T1/T2 pair when using reference annotations for 0% of target data and various fractions (1%, 10%, 40%, 70% and 100%) of source data during training. For readability, standard deviations across the runs are not shown.

Reaching supervised performance. M-GenSeg provides encouraging improvements on the target modality as compared to a supervised method trained on source data without domain adaptation, as shown in Fig. 3. However, when no reference annotations are provided for the target modality, the performance does not reach the one from fully supervised methods trained on the fully annotated target modality. It is thus beneficial to determine the fraction of target modality annotations required to match fully supervised performance. Fig.4 shows the Dice difference between UAGAN, and AttENT, AccSegNet, M-GenSeg with 100% source annotations and increasing fractions of target

annotations (0%, 10% and 20%). We report in average an absolute Dice difference on target modality of 0.021 from T2 to T1 and 0.02 from T1 to T2 between UAGAN trained with all labels and our method trained with all source images annotated and 20% of the target images annotated. Thus, the annotation burden could be reduced with the M-GenSeg method.

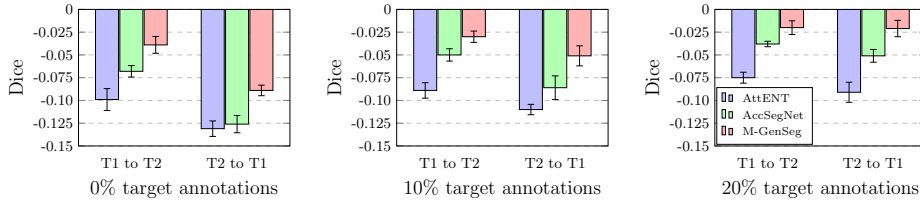


Fig. 4: Dice difference on target modality, as compared to the fully supervised method UAGAN, when using T1/T2 reference annotations for 100% of source data and increasing fractions of target data (0%, 10% and 20%). A gap of 0 means that fully supervised method performance has been reached.

3.3 Ablation Experiments

The following ablation tests, conducted to validate the conception choices and presented in Fig. 7a and Fig. 7b, were run on six different domain adaptation experiments (T1 to T2, T1 to FLAIR, T1 to T1ce and vice-versa) where all the target modality images are unannotated. The variability across the different modality pairs explain the high standard deviations reported in Fig. 7a and 7b.

Attention-aware generators. To validate the use of the attention gates in the skip connections, we evaluated the performance of M-GenSeg with different shortcut variants. Fig. 7b shows the performance with concatenation, skinny cat [10] and summation skip connections relatively to the performance of the proposed variant with attention gates. Though they provide only a slight performance gain, attention gates have the benefit to give insight on what happens in the model. Fig. 6 shows the attention maps generated for each type of decoder. As expected, residual decoders focus towards tumor areas. More interestingly, in order not to disturb the process of healthy image generation, common decoders avoid lesion locations. Finally, modality translators tend to focus on salient details of the brain tissue, which facilitates contrast redefinition needed for accurate translation.

Modality invariant features. Some unsupervised cross-modality translation models [4,8,15,14] rely on modality invariant features to perform their image-to-image translation. To do so, additionally to the $m \rightarrow m' \rightarrow m$ CycleGan translation objective, they introduce an identity loss such that $m \rightarrow m$ self-reconstruction can be achieved after encoding and decoding. In our case, this loss could be written $\mathcal{L}_{idt}^{mod} = \sum_{\substack{m \in \{S,T\} \\ b \in \{A,P\}}} \mathcal{L}_1([G_m \circ E_m](\mathbf{x}_b^m), \mathbf{x}_b^m)$ and imposes

that an image \mathbf{x}_b^m remains in the same modality m when sequentially going through the encoder and modality decoder specific to this modality, E_m and G_m . We tested this loss with M-GenSeg and different choices of λ_{idt}^{mod} , but did not observe performance gains. We thus believe such a loss is unnecessary here.

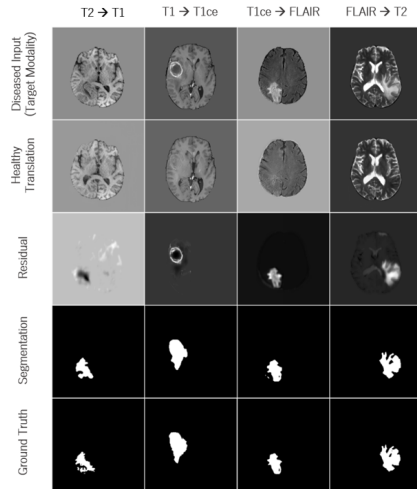


Fig. 5: Examples of image translation from Presence to Absence domains and resulting segmentation in different adaptation experiments. Each column represents a domain adaptation scenario. For each instance, the input image considered belongs to target modality data, which had no pixel-level annotations provided.

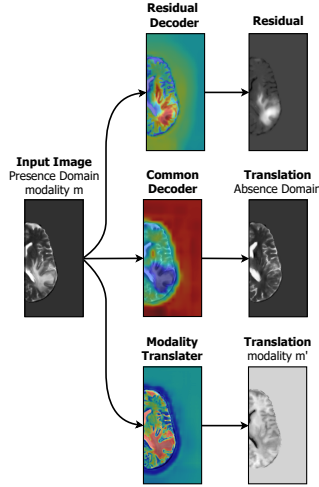


Fig. 6: Attention maps for Presence \rightarrow Absence and modality translations. Red color indicates areas of focus while dark blue correspond to locations ignored by the network.

Image-level supervision. To assess the value of the image-level supervision in this domain adaptation context, we tried M-GenSeg without any GenSeg unsupervised objective. In other words, all λ^{Gen} loss components were set to 0. As expected, the source modality segmentation performance wasn't impacted, however segmentation accuracy on the target modality dropped, implying that the use of image-level labels is helpful.

Translations for healthy data. We conjecture that training modality translation only on diseased data is sufficient. However, doing it for healthy data as well provides additional training examples for this task, which is reflected in the performance. Likewise, performing translation from absence to presence domain is not necessary, but yields better Dice scores by making more efficient use of the data. Finally, training M-GenSeg without any healthy path at all (both previous experiments combined) gave even worse Dice scores. We thus claim that healthy tissues, if adequately incorporated to the training process of neural networks like in M-GenSeg, can help to better delineate tumor lesions in segmentation tasks. Note that feeding healthy tissues to supervised methods (along with empty masks) does not suffice, as it only helps to reduce false positives. Indeed, we trained a TransUnet model with either only diseased or both diseased and healthy data. The latter yielded a higher dice score (0.867 ± 0.04 vs 0.836 ± 0.014) and precision (0.878 ± 0.005 vs 0.803 ± 0.017) in comparison to using only diseased examples. However, the trade-off is a lower recall (0.856 ± 0.008 vs 0.873 ± 0.009) which makes it more prone to miss some lesions.

Unshared latent space. We contend that image-level supervision and modality translation benefit from sharing their latent representations. We thus evaluated M-GenSeg with separate latent spaces for these two tasks, which simply requires duplicating the encoders. The drop in performance for this variant indicates that M-GenSeg efficiently combines both tasks when the latent representations share model updates.

Residual/Segmentation separation. Finally, we tried using a separate segmentation decoder instead of sharing the residual and segmentation weights. As for GenSeg [10], the separate version under-performed on the brain dataset. This further highlights that disentangling tumors from the background to perform diseased to healthy translation is helpful for tumor segmentation, particularly on the target modality.

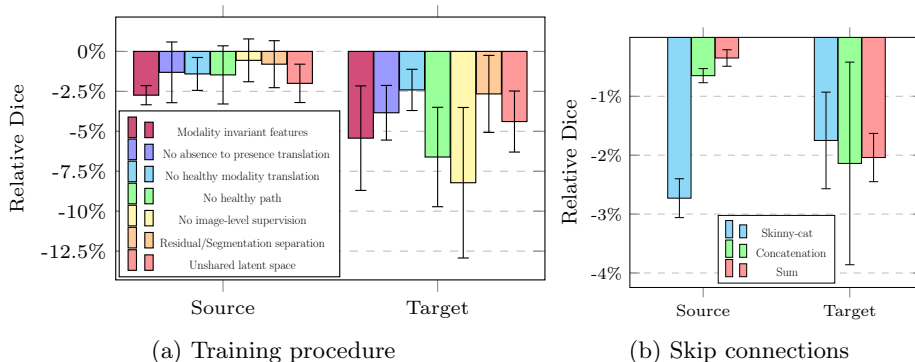


Fig. 7: Ablation studies : relative Dice change on source and target modalities, as compared to the full version of the proposed model. X% relative value means that the ablation reached 100%+X% of complete M-GenSeg Dice performance. Therefore negative values indicate that the ablation led to decrease in performance.

4 Conclusion

In this study, we propose a M-GenSeg, a new framework for unpaired cross-modality medical image segmentation when the target modality is unannotated or partially annotated. As this is a semi-supervised method, we also support scenarios where only a fraction of the source modality is annotated. Specifically, we combined two unsupervised image-to-image translations to perform both modality adaptation and leverage image-level labels, the latter being much easier to obtain than pixel-level annotations. Experiments showed that in domain-adaptive segmentation tasks, our method outperforms state-of-the-art models, while yielding robust performance even when a small fraction of the source images is annotated. We therefore contend that M-GenSeg is an annotation-efficient framework that greatly reduces the performance gap due to domain shift in cross-modality tumor segmentation. Pending increased computing resources, future work will explore the use of full 3D images rather than 2D slices, along with larger and more optimal architectures.

References

1. L. M. Prevedello, S. S. Halabi, G. Shih, C. C. Wu, M. D. Kohli, F. H. Chokshi, B. J. Erickson, J. Kalpathy-Cramer, K. P. Andriole, and A. E. Flanders, “Challenges related to artificial intelligence research in medical imaging and the importance of image analysis competitions,” *Radiology: Artificial Intelligence*, vol. 1, no. 1, p. e180031, 2019.
2. H. Guan and M. Liu, “Domain adaptation for medical image analysis: A survey,” *IEEE Trans. Biomed. Eng.*, no. 3, pp. 1173–1185, 2022.
3. C. Pei, F. Wu, and L. Huang, “Disentangle domain features for cross-modality cardiac image segmentation,” *Medical Image Analysis*, vol. 71, p. 102078, 2021.
4. C. Li, X. Luo, W. Chen, Y. He, M. Wu, and Y. Tan, “Attent: Domain-adaptive medical image segmentation via attention-aware translation and adversarial entropy minimization,” in *2021 IEEE International Conference on Bioinformatics and Biomedicine (BIBM)*. IEEE, 2021, pp. 952–959.
5. Y. Huo, Z. Xu, H. Moon, S. Bao, A. Assad, T. K. Moyo, M. R. Savona, R. G. Abramson, and B. A. Landman, “Synseg-net: Synthetic segmentation without target modality ground truth,” *IEEE Transactions on Medical Imaging*, vol. 38, no. 4, pp. 1016–1025, 2019.
6. C. Chen, Q. Dou, H. Chen, J. Qin, and P.-A. Heng, “Synergistic image and feature adaptation: Towards cross-modality domain adaptation for medical image segmentation,” vol. 38, 2019, pp. 865–872.
7. J. Jiang, Y.-C. Hu, N. Tyagi, C. Wang, N. Lee, J. O. Deasy, B. Sean, and H. Veeraraghavan, “Self-derived organ attention for unpaired CT-MRI deep domain adaptation based MRI segmentation,” *Phys. Med. Biol.*, vol. 65, no. 20, p. 205001, 2020.
8. B. Zhou, C. Liu, and J. S. Duncan, “Anatomy-Constrained Contrastive Learning for Synthetic Segmentation Without Ground-Truth,” in *Medical Image Computing and Computer Assisted Intervention*. Springer, 2021, vol. 12901, pp. 47–56.
9. J.-Y. Zhu, T. Park, P. Isola, and A. A. Efros, “Unpaired Image-to-Image Translation Using Cycle-Consistent Adversarial Networks,” in *2017 IEEE International Conference on Computer Vision (ICCV)*. IEEE, 2017, pp. 2242–51.
10. E. Vorontsov, P. Molchanov, M. Gazda, C. Beckham, J. Kautz, and S. Kadoury, “Towards annotation-efficient segmentation via image-to-image translation,” *Medical Image Analysis*, vol. 82, p. 102624, 2022.
11. M. Drozdal, E. Vorontsov, S. Kadoury, and C. Pal, “The Importance of Skip Connections in Biomedical Image Segmentation,” in *Deep Learning and Data Labeling for Medical Applications*. Springer, 2016, vol. 10008, pp. 179–187.
12. O. Oktay, J. Schlemper, L. L. Folgoc, M. Lee, M. Heinrich, K. Misawa, K. Mori, S. McDonagh, N. Y. Hammerla, B. Kainz, B. Glocker, and D. Rueckert, “Attention U-Net: Learning Where to Look for the Pancreas,” 2018.
13. J. Chen, Y. Lu, Q. Yu, X. Luo, E. Adeli, Y. Wang, L. Lu, A. L. Yuille, and Y. Zhou, “TransUNet: Transformers Make Strong Encoders for Medical Image Segmentation,” 2021.
14. W. Yuan, J. Wei, J. Wang, Q. Ma, and T. Tasdizen, “Unified Attentional Generative Adversarial Network for Brain Tumor Segmentation from Multimodal Unpaired Images,” in *Medical Image Computing and Computer Assisted Intervention*. Springer, 2019, vol. 11766, pp. 229–237.
15. W. Xia, Y. Yang, and J.-H. Xue, “Unsupervised multi-domain multimodal image-to-image translation with explicit domain-constrained disentanglement,” *Neural Networks*, vol. 131, pp. 50–63, 2020.